Dalton Transactions

PAPER

View Article Online
View Journal | View Issue

Cite this: *Dalton Trans.*, 2017, **46**, 10899

Control over cyclisation sequences of 1,1′-bifunctional octamethylferrocenes to ferrocenophanes†

Max Roemer,*[a] Duncan A. Wild,[a] Brian W. Skelton,[a,b] Alexandre N. Sobolev,[b] Gareth L. Nealon,[b] Matthew J. Piggott[a] and George A. Koutsantonis*[a]

Received 5th June 2017,
Accepted 18th July 2017

DOI: 10.1039/c7dt02037f

rsc.li/dalton

This paper describes the facile synthesis of a number of electron rich octamethyl[1.4]ferrocenophanes with unsaturated handles from 1,1′-bis(1-chlorovinyl)octamethylferrocene. Treatment of this reactive compound with sodium hydroxide in DMF initiates a series of reactions resulting in the formation of four different ferrocenophanes. The most complex of these products arises from a cascade of cyclisations giving an unusual, unsymmetrical bis-ferrocenophane with a central fused cyclobutene. Control over the reaction outcome is achieved by manipulating the concentration of NaOH. Mechanisms are proposed, and supported by DFT calculations.

Introduction

Ferrocenophanes, organometallic analogues of cyclophanes, are an important class of ferrocenes, which find application in polymer and materials science,[1,2] electrochemistry,[3] medicine,[4,5] and sensors.[6] The bridge(s) connecting cyclopentadienyl (Cp) rings inhibit rotation around the metal and may induce a ring tilt, which can alter the chemical and physical properties of ferrocenes remarkably, compared to their non-bridged counterparts. A broad variety of ferrocenophanes have been reported, including those with all-carbon[7] and hetero element-containing bridges.[2,8–10] Only a single report mentions formation of an all-carbon-bridged bis-ferrocenophane with fused handles bearing a 4-membered ring.[11] Unbridged ferrocenes have been connected by cycloaddition reactions of trifluorovinylferrocenes[12,13] and a chloroferrocenyl allene[14] that give four-membered rings in the linker. Several 1,1′-ethenyl ferrocenes have been found to cyclise to [1.4]ferrocenophanes.[12,15–17]

Highly methylated ferrocenes are important in many fields; however, their chemistry is significantly less explored than that of their non-methylated counterparts. The lower oxidation-potentials in the more electron-rich methylated ferrocenes can result in surprising reactivity, for instance, the attainment of the Fe(IV) oxidation state.[18] Methyl groups also greatly enhance solubility, making highly methylated ferrocenes valuable building blocks in larger molecular scaffolds. Surprisingly, octamethylferrocene-based ferrocenophanes have received very little attention. Formation of such compounds was described from a 1,1′-diethynyloctamethylferrocene derivative,[19] by metathesis of a 1,1′-alkenyl precursor,[20] and we recently reported on the formation of **4** from **1**, Scheme 1.[21]

Results and discussion

In this work we use 1,1′-bis(1-chlorovinyl)octamethylferrocene (**1**) to provide access to octamethylferrocenophanes, *viz.* a tricyclic

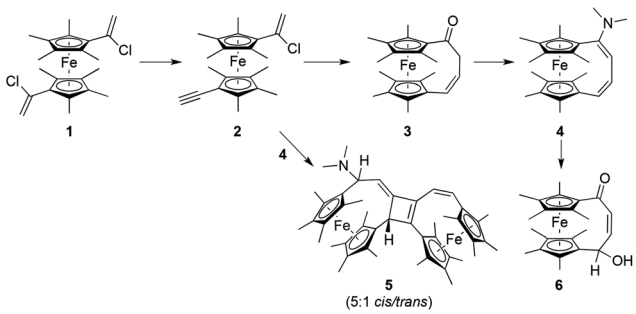

Scheme 1 Reaction of compound **1** leading to an array of ferrocenophanes. The product distribution can be controlled by adjusting the NaOH concentration. Conditions: 45 min/60 °C; DMF/aq. NaOH (0.75 M) in a ratio of 3 : 1 for isolation of **4**, and 6 : 1 for isolation of *cis*/*trans*-**5**.

[a]*Chemistry, School of Molecular Sciences, University of Western Australia, 35 Stirling Hwy, Crawley, WA 6009, Australia. E-mail: max.roemer@uwa.edu.au, george.koutsantonis@uwa.edu.au*
[b]*Centre for Microscopy, Characterisation and Analysis, University of Western Australia, Crawley, Western Australia 6009, Australia*

†Electronic supplementary information (ESI) available: NMR spectra, and cyclic voltammograms. Molecular graphics were prepared using OLEX2.[30] Full experimental details and crystallographic information files in cif-format. CCDC 1528955–1528957 for compounds **3**, *cis*-**5** and **6**. For ESI and crystallographic data in CIF or other electronic format see DOI: 10.1039/c7dt02037f

bis[1.4]ferrocenophane (**5**), and several other mononuclear ferrocenophanes (Scheme 1). The formation of these products can be explained by initial dehydrohalogenation of **1** to alkyne **2** in DMF/NaOH, followed by cyclisation to give **3**. Methylamine, generated *in situ* from base-induced hydrolysis of DMF, reacts with ketone **3** to form the enamine **4**. Using a high concentration of NaOH leads to fast and quantitative formation of **4**.[21] Intriguingly, by lowering the concentration of NaOH, the *cis* and *trans* cyclobutenes **5** become the major products.

The product distribution depends on several factors, including the concentration of NaOH, reaction temperature and time. The conditions can be tuned to afford either **4** or **5** as the major products, with **3** and **6** isolated as minor by-products. The formation of **5** proceeds diastereoselectively, affording a mixture of the *cis*- and *trans* isomers in a ~5 : 1 ratio. The ferrocenophanes **4** and **5** are sensitive towards standard chromatographic supports, which made optimisation of the reaction and the development of a chromatography free work-up essential. After some experimentation, we found that **5** can be purified by repeated washings with DMF, affording the isomeric mixture free from impurities, as judged by ^{1}H NMR spectroscopy.

We were able to characterise *cis*-**5** unambiguously by NMR spectroscopy. Due to its asymmetry, all 18 methyl groups in *cis*-**5** give rise to individual resonances in the ^{1}H NMR spectrum (Fig. S16†), and each *ipso*-carbon gives a single resonance in the ^{13}C NMR spectrum (Fig. S18†). The resonances due to the fused handle were assigned with the aid of 2D NMR techniques (ESI†) and evaluation of coupling constants. The three vinylic protons each give rise to individual apparent doublet of doublets in the ^{1}H NMR spectrum, with ^{3}J(H–H) coupling constants of 12.3 Hz for the *cis* coupling and 4.7 Hz for the allylic coupling. Each vinylic signal shows further long range couplings to the cyclobutenyl proton, observed in the 2D spectra but not adequately resolved.

X-ray crystal structures of all ferrocenophanes were obtained (Fig. 1 and 2). The tilt angles α, the dihedral angles between both Cp rings (Fig. 3A[2,8]), and the twist angles β (Fig. 3B), the average value of the torsion angles between Cp-C atoms and centres of the Cp rings (Fig. 3B) are compared in Table 1. The Cp rings of the cyclophanes **3**, *cis*-**5** and **6**, which are attached to a handle with only one double bond, are essentially parallel with tilt angles $\alpha < 1°$ (Fig. 3). This value is small compared to other (non-methylated) [1.4]ferrocenophanes,[12,16,19] and presumably is a result of steric repulsion between the methyl groups resisting tilting. The two crystallographically different molecules of **4** and the ferrocenophane frame of *cis*-**5** bearing two double bonds are tilted slightly more (1.42–2.97°), which is attributed the rigidity of the unsaturated linker. The observed Cp twist β ranges from 1.8° to 33.8°; again the handles with two double bonds (**4**, *cis*-**5**) induce the minor twist in the molecule. Tilt and twist angles (Fig. 3) are summarised in Table 1. The cyclobutene ring of *cis*-**5** is slightly puckered with an average torsion angle of 5.0(6)°.

We studied the role of NaOH by varying its concentration in the reaction mixture, which revealed that the base is involved

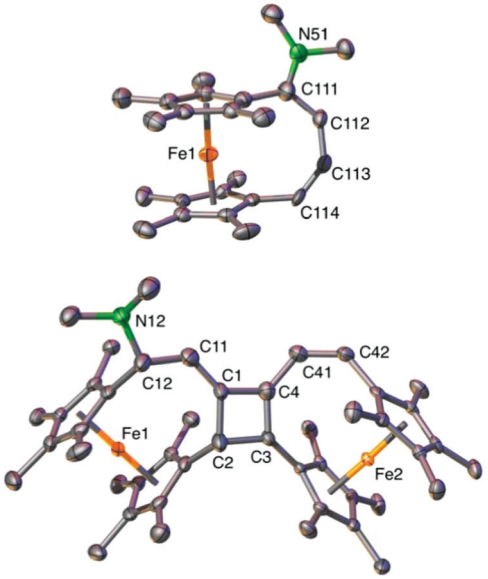

Fig. 1 Representation of the molecular structures of ferrocenophanes **4** (top) and *cis*-**5** (bottom), as determined by X-ray single crystal diffraction. H-Atoms are omitted for clarity and major components of the disordered fragments are illustrated. Atomic displacement ellipsoids are shown at probability level of 30%.

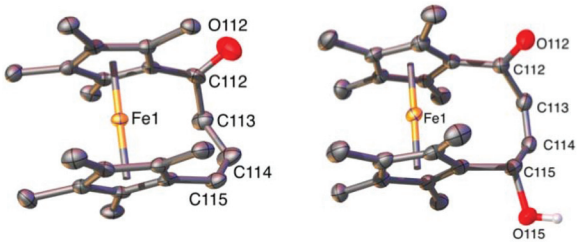

Fig. 2 Representation of the molecular structures of ferrocenophanes **3** (left) and **6** (right), as determined by X-ray single crystal diffraction. H-Atoms are omitted for clarity. Atomic displacement ellipsoids are shown at a probability level of 30%.

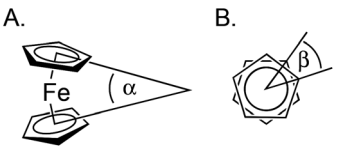

Fig. 3 Tilt (α) and twist (β) angles of the ferrocenophanes. For determination of β, we used the average of the torsion angles between the centers of both Cp rings, and each set of C atoms giving the smallest angle.

in several processes: firstly, generation of alkynes through the dehydrohalogenation of the chlorovinyl groups; secondly, substitution of the remaining vinyl chloride, followed by cyclisation to form **3**; and lastly, base-induced hydrolysis of the DMF to give dimethylamine.[22] A high concentration of NaOH results in the rapid generation of **2**, cyclisation to **3**, and sub-

Table 1 Tilt and twist angles of the Cp rings

Compound	Cp tilt α/°	Cp twist β/°
3	0.79 (10)	4.36(3)
4 (Molecule 1)	2.97(4)[a]	17.96(4)[a]
4 (Molecule 2)	1.42(4)[a]	22.34(6)[a]
cis-**5**	0.71(17)[b]/2.27(13)[c]	1.84(5)[b]/33.84(4)[c]
6	0.85 (14)	7.52(4)

Compound **4** crystallises with two molecules in the asymmetric unit, which both consist of two disordered fragments. [a] Values quoted for the major component only. [b] Fc frame at Fe1. [c] Fc frame at Fe2.

sequent transformation to **4** by reaction with Me_2NH, produced by fast decomposition of DMF (Scheme 1). On the contrary, a low concentration of NaOH slows these processes down, allowing other pathways to compete. The transformation was investigated using a 4 mM solution of **1** in DMF and varying concentrations of NaOH. Fig. 4 shows the composition of each crude product, determined by ^{1}H NMR spectroscopy after aqueous work-up (ESI, S5, S7–11†). Low concentrations of NaOH afforded significant quantities of unreacted **1**, together with an intermediate identified by ^{1}H NMR spectroscopy and mass spectrometry as 1-(1-chlorovinyl)-1′-(ethynyl)octamethylferrocene (**2**). The proportion of **3** produced peaked at a moderate NaOH concentration (exp. B). With increasing concentration of NaOH, the proportion of **5** rises, but then plateaus (exps C/D). By increasing the concentration of NaOH further, it decreases again and enamine **4** becomes the major product (red bars, Fig. 4).

Under optimised conditions an isolated yield of 39% of **5** (62% yield by ^{1}H NMR spectroscopy), was obtained, but formation of **4** could not be avoided. Enyne **2** can be obtained under anhydrous conditions by treatment with ^{t}BuOK, but is accompanied by 1,1′-diethynyloctamethylferrocene (ESI, Fig. S13 and S19†). Preparation of phenylacetylene from 1-chlorostyrene is well known,[23] and analogous reactions have been reported with chlorovinyl ferrocenes.[24] Filtration of the mixture of enyne **2** and the diethynyl derivative though a pad of Al_2O_3 led to cyclisation of **2** to give ferrocenophane **3**, suggesting that **2** is the precursor for **3**. Compound **3** is known to form from the silica gel-induced decomposition of a ferrocenophane bearing a 1-methoxy-1,3-butadiene handle;[19] however, its solid state structure (Fig. 2) remained hitherto undetermined.

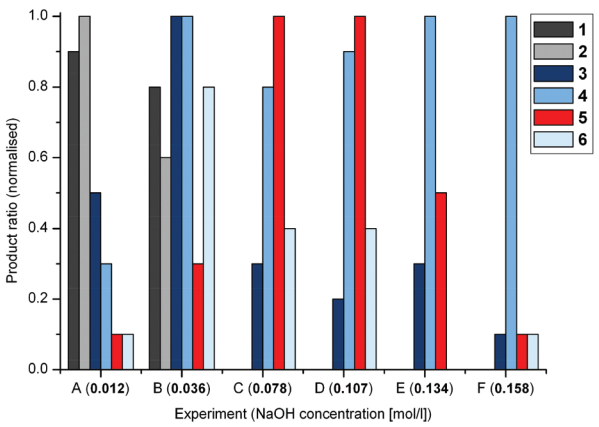

Fig. 4 Product distribution among compounds **1–6** for the base-induced transformation of **1** to ferrocenophanes, as determined by ^{1}H NMR spectroscopy. Each distribution is normalised against the most abundant product for that experiment. Conditions: 10 mg **1** in 6 ml DMF (~4 mM); varying amount of 0.75 M NaOH: 0.1 ml (A), 0.3 ml (B), 0.7 ml (C), 1.0 ml (D), 1.3 ml (E), 1.6 ml (F) resulting in the overall NaOH concentration reported in brackets.

Subsequently, the reactivities of the isolated complexes were investigated to help shed light on the mechanism of the formation of the most complex products **5**. Compounds **5** were not obtained from heating **1** and **4** together, either neat or in a DMF solution. Consequently, the reaction of **1** and **4**, or the dimerisation of **4**, followed by elimination of dimethylamine, can be ruled out as a possible pathway to **5**. We further investigated the reaction of **1** in DMF-d_7, with NaOD in D_2O, which resulted in the fast deuteration of the chlorovinyl groups of **1**. After prolonged exposure, the ^{1}H NMR spectrum indicated complete deuteration of the handle protons of ferrocenophanes formed, giving no mechanistic insights.

Based on our experiments and the results of density functional theory (DFT) calculations, we formulate a possible reaction mechanism involving a cascade of three cyclisation reactions, depicted in Fig. 5. The first cyclisation, path A, is initiated by an S_N1 reaction of hydroxide and **2** generated *in situ*, facilitated by the electron-rich octamethylferrocene. Deprotonation generates the enolate, which undergoes intramolecular addition to the adjacent alkyne, generating the ferrocenophane **3**. Similar cyclisations of *ortho*-alkynylacetophenones have been described.[25] On the basis of the DFT calculations we revise our previously proposed mechanism for the formation of **4**,[21] and now suggest that **3** forms initially and is converted into **4** in the presence of Me_2NH generated *in situ* from base-induced hydrolysis of DMF. As we noted previously, the formation of an enamine under aqueous conditions is somewhat surprising, but not without precedent in conjugated systems.[26] The formation of bis-ferrocenophanes **5** (*cis* isomer only shown) can be rationalised by two further cyclisations involving **2** and **4** (Fig. 5B). Initially, a [2 + 2]-cycloaddition of the terminal alkyne of **2** and the butadiene handle of **4** affords cyclobutene B2, with the *cis*-configuration expected from cycloaddition. Notably, both reaction partners are electron rich, and the reaction does not involve a catalyst;[27,28] nevertheless, the transformation is exothermic (B1 → B2, Fig. 5D). The reaction occurs regioselectively at C3═C4, which is possibly due to steric hindrance at C1 (Fig. 8). Elimination of HCl from the remaining chlorovinyl group in B2 presumably occurs next; if it occurred prior, the diethynylferrocene would be expected to undergo intramolecular cyclisation under basic conditions.[19] Ring-opening of B3 to give B4, followed by a base-induced conjugate addition/ring-closing affording B5, was energetically the most feasible mechanism of several investigated. Other mechanisms in which the cyclobutene moiety is retained give much higher energy intermediates, by ~150 kJ mol^{-1}. Calculations

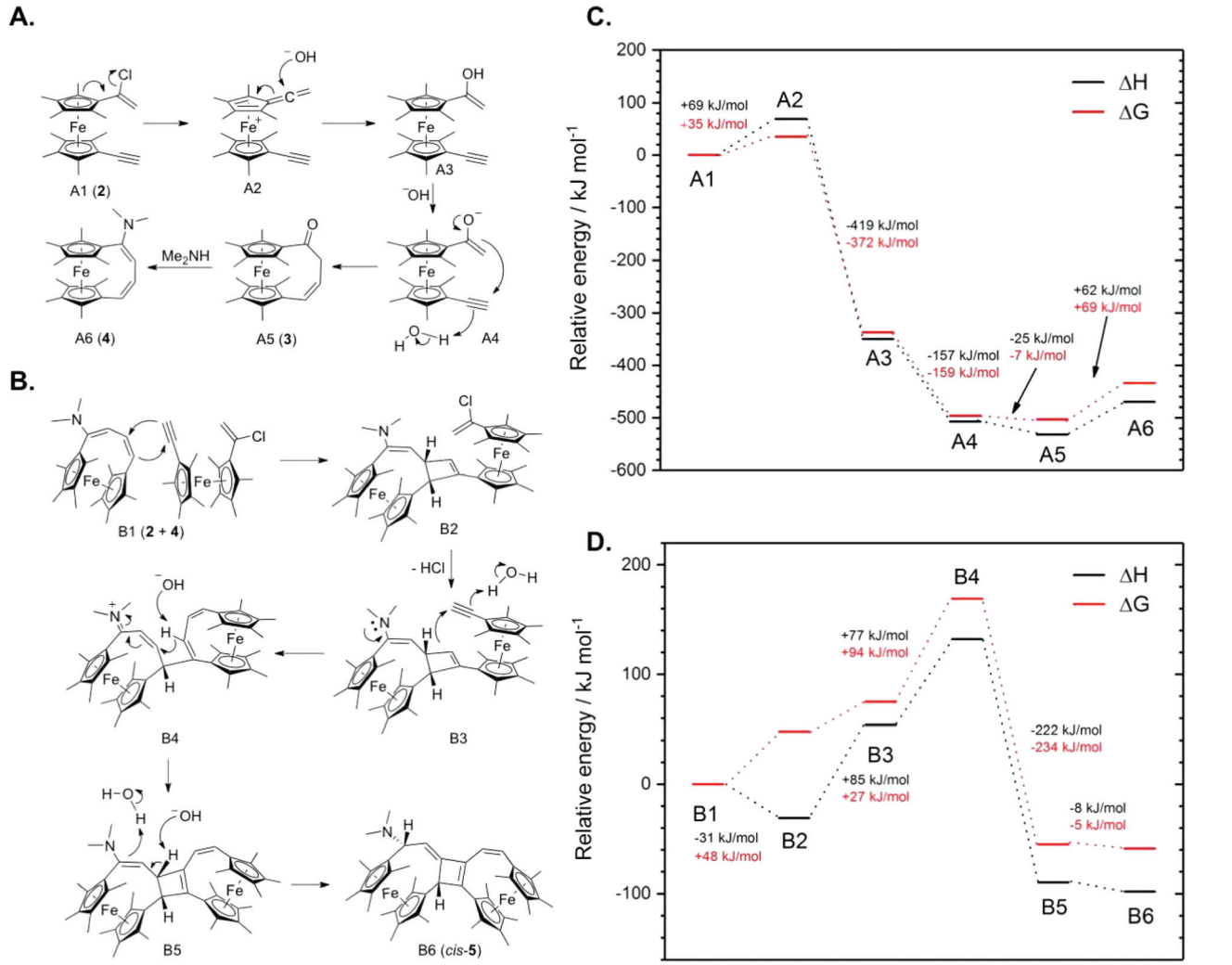

Fig. 5 A. Proposed mechanism for cyclisation of **2** to **3** and transformation to enamine **4** by reaction with Me_2NH. B. The multistep cascade of reactions leading to **5**. C. Calculated reaction energies determined by DFT calculation for all intermediates in the proposed mechanism A. D. Calculated reaction energies determined by DFT calculation for all intermediates in the proposed mechanism B.

support the notion that the newly formed stereocentre in B5 has the relative configuration indicated as this has the lower energy. Base-catalysed tautomerisation of B5 then gives the more thermodynamically stable product *cis*-**5**, along with a little of the *trans*-isomer. Fig. 5C and D summarise the computed enthalpy and free energy changes for the reactions, with the starting point of each scheme set at 0 kJ mol^{-1}. The calculations reveal that the proposed mechanism is energetically feasible, with the reaction being overall exothermic and exergonic. This sequence of events can only occur when sufficient quantities of **2** and **4** are present, explaining the absence of **5** when higher concentrations of NaOH are used. We also computationally investigated an alternative mechanism involving cyclisation of 1,1′-diethynyloctamethylferrocene (Scheme S1, ESI†). Cyclisation of this compound is energetically feasible (Table S1†), and has also been reported.[19] Therefore, we cannot exclude that minor amounts of this compound form during the reactions, which cyclise to afford the same products. Nevertheless, as described above, application of isolated **2** to silica yielded **3**. Due to the slightly acidic nature of silica, we can rule out transformation of the one chlorovinyl group into an alkyne, which in turn means that **2** is indeed the intermediate which cyclises, at least under these conditions.

We tested several water/NaOH/solvent (THF, MeOH, DMSO, ^{t}BuOH) systems, and found that efficient cyclisations occur exclusively in DMF/H_2O/NaOH, which may reflect its superior ability to stabilise polar transition states.

Complex **3** also forms in the absence of NaOH, but only in low yield as hydrolysis of the chlorovinyl group to give the methyl ketone competes.[21]

Surprisingly, reaction of enamine **4** in ^{t}BuOH/H_2O in air produces ferrocenophane **6** in a yield of 56%, with no evidence for other ferrocenophane products (Scheme 2). In contrast, using degassed solvents under Ar did not induce any transformation. The formation of **6** must involve oxidation of **4** or an intermediate, which is likely triggered by trace oxygen. Only

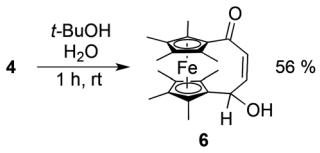

Scheme 2 Reaction of **4** to ferrocenophane **6** under aqueous conditions in air.

this oxidation enables nucleophilic addition of water. This also provides an explanation for the varying amounts of **6** in the above discussed transformations of **4** in DMF/NaOH. All reactions were performed under Ar in air-free solvents but the work-up was conducted in air. The fact that **4** and **6** were detected in all reactions, with the exception of *E*, and that **4** has been unambiguously shown to be the precursor for **6**, indicates that **6** forms as decomposition product of **4** during work-up of the reactions. There are some examples of ferrocenophanes with [1.4]diketo-handles[12,16] but, to the best our knowledge, the handle that **6** bears is unprecedented. Compound **1**, heated in a mixture of DMF/H_2O, afforded the hydrolysis product 1,1′-diacetyloctamethylferrocene as the major product, and significant quantities of ferrocenophane **3**, but no **6**.

We studied the redox behaviour of the ferrocenophanes by cyclic voltammetry. Oxidation potentials are summarised in Table 2. Compound **4** oxidises at the remarkably low potential of −425 mV.[21] This redox process is only reversible if the cathodic peak potential is kept low (*i.e.* ∼−160 mV), as higher potentials induce decomposition. Fig. 6 shows the cyclic voltammogram (CV) of **5**, exhibiting two well resolved redox-processes $E_{1/2}(1)$ = −315 mV and $E_{1/2}(2)$ = −113 mV, with a splitting $\Delta E(1–2)$ of 202 mV. The first oxidation is elevated by 110 mV, compared to that of **4** (−425 mV (ref. 21)).

Based on DFT calculations, the HOMO of *cis*-**5** is metal-centred, situated at the Fc bearing the Me_2N-moiety in the α-position (Fig. 7). Thus, the first oxidation is assigned to this Fc and subsequent oxidation at the remaining Fc. The reversible redox behaviour of **5** indicates that no oxidation takes place at the dimethylamino group, which in turn suggests that oxidative decomposition of **4** is not related to oxidation of that group. The cyclic voltammograms of compounds **3** and **6** show a reversible process at −285 mV and −32 mV, respectively, which are well above those of **4** and **5**, due to the presence of the electron withdrawing carbonyl. The ratio of anodic and

Table 2 Oxidation potentials determined by cyclic voltammetry. All potentials are reported *vs.* the Fc/Fc^+ redox couple. Measurements were conducted in CH_2Cl_2 using Bu_4NPF_6 as the supporting electrolyte (0.1 M)

Compound	$E_{1/2}(1)$ [mV]	$E_{1/2}(2)$ [mV]	ΔE [mV]
3	−285	—	—
	−150[a]		
4	−425	—	—
5	−315	−113	202
6	−32	—	—

[a] Conducted in MeCN using $NaClO_4$ as supporting electrolyte.[19]

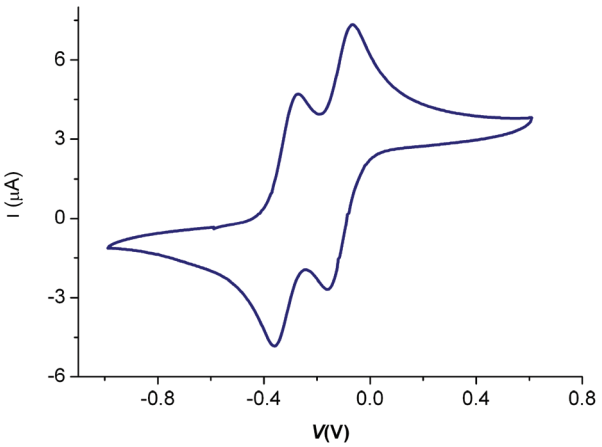

Fig. 6 Cyclic voltammogram of **5**, *vs.* the Fc/Fc^+ redox couple. Conditions: 1 mM analyte concentration in DCM, supporting electrolyte 0.1 M Bu_4NPF_6, scan rate 100 mV s^{-1}.

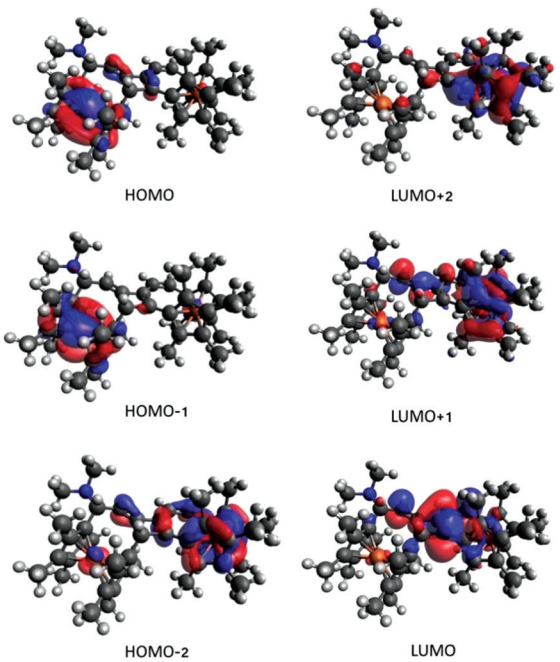

Fig. 7 Frontier orbitals of *cis*-**5** obtained by DFT calculations.

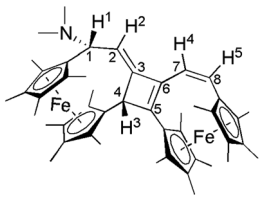

Fig. 8 NMR numbering scheme for the handle system of the bis-ferrocenophane *cis*-**5**.

cathodic peak current (i_{pa}/i_{pc}) was close to unity and independent of the scan rate (Fig. S1–S4†), as expected for reversible redox processes.[29]

Conclusions

In conclusion, we have shown the base induced reactions of 1,1′-bis(1-chlorovinyl)octamethylferrocene **1**, in DMF, affords a variety of ferrocenophanes with only minor changes in reaction conditions. Detailed investigation of the complex system by varying stoichiometry influenced the product distributions, and in conjunction with control experiments and DFT calculations, allowed plausible mechanisms for the formation of most of the observed products to be proposed. The electron-donating ability of the octamethylferrocene moieties play an important role in some of the mechanistic steps. The unusual transformations described in this work demonstrate the rich chemistry of octamethylferrocenes and suggests that future use of this moiety will be equally fertile.

General

Reactions were performed under Ar atmosphere using standard Schlenk techniques unless otherwise stated. *N*,*N*-Dimethylformamide (DMF) was distilled from CaH_2. THF was distilled from sodium/benzophenone. 1,1′-Bis(1-chlorovinyl)-octamethylferrocene (**1**) and complex **4** were prepared as previously described.[21] Other compounds were purchased from Sigma–Aldrich. Cyclic voltammetry was conducted on a Princeton Applied Research VersaSTAT 3 potentiostat using a three electrode setup with Pt working electrode, and Pt coated titanium rods as counter and pseudo-reference electrodes. NMR spectra were recorded on Bruker AV500 and AV600 spectrometers. Chemical shifts of solvent signals were used to reference the spectra internally.[31] Mass spectra were recorded on a Waters LCT Premier mass spectrometer in ESI^+ and $APCI^+$ modes. Elemental analyses were obtained from the Elemental Analysis Service of the London Metropolitan University. Infrared spectra were recorded on a PerkinElmer Spectrum One FT-IR spectrometer equipped with an ATR sampling accessory. Melting points were determined using a Reichert melting point microscope.

Syntheses

Optimisation reactions for preparation of (*cis*/*trans*)-5. 1,1′-Bis(1-chlorovinyl)octamethylferrocene (**1**) (10 mg, 0.024 mmol, experiments A–F; 20 mg, 0.048 mmol, experiment G) was dissolved in DMF (6 ml) in a Schlenk tube. NaOH solution (0.75 M) was added according to Fig. 4. The reaction mixtures were heated for 45 min to 60 °C with stirring and subsequently cooled to 0 °C. Dilution with water (15 ml) resulted in the formation of a precipitate. Experiments C, D and G produced a pale pink precipitate, with the amount of precipitate increasing in the order C < D < G. The suspension was extracted with dichloromethane (50 ml). The organic phase was washed with water (2 × 50 ml), dried over Na_2SO_4 and evaporated under high vacuum with gentle heating, affording a red-orange mixture, which was analysed by ^{1}H NMR spectroscopy (Fig. S3, S5 and S7–S12†). Experiments A and B yielded, in addition to compounds **1**, **3**, **4**, **5** and **6** substantial amounts of compound **2**. Fig. S6† shows the mass spectrum of the mixture. The mass 406 corresponds to $[\mathbf{2} + Na]^+$.

2: Compound **1** (10 mg, 0.024 mmol) was dissolved in THF (6 ml) and cooled to 0 °C. ^{t}BuOK (9 mg, 0.07 mmol) was added. The cooling bath was removed, and stirring was continued for 30 min. Additional ^{t}BuOK (9 mg, 0.07 mmol) was added and the mixture was stirred for 1 h. The solvent was removed under vacuum and the residue was dissolved in C_6D_6, affording a bright orange solution, which was analysed by ^{1}H NMR spectroscopy. The ^{1}H NMR spectrum shows signals of starting material **1**, intermediate **2**, and 1,1′-diethynyloctamethylferrocene (Fig. S13†). After standing for 2 h, the solution darkened significantly and the ^{1}H NMR spectrum showed compounds **1** and **2** to be intact but no traces of 1,1′-diethynyloctamethylferrocene. Filtration of the solution through a pad of neutral alumina afforded a mixture of **1** and **2** from the first fraction eluted with hexane, and compound **3** from the second fraction eluted with EtOAc. Spectroscopic data for **2**: ^{1}H NMR (600 MHz, C_6D_6, 25 °C): δ = 5.78 (d, ^2J = 0.7 Hz, 1H, =CH_2), 5.72 (d, ^2J = 0.7 Hz, 1H, =CH_2), 2.73 (s, 1H, C≡C*H*), 1.86 (s, 6H, CH_3), 1.81 (s, 6H, CH_3), 1.60 (s, 6H, CH_3), 1.52 (s, 6H, CH_3) ppm.

5: Compound **1** (100 mg, 0.24 mmol) was dissolved in DMF (30 ml). Degassed aqueous NaOH solution (0.75 M; 5 ml) was added and the solution was stirred at 60 °C for 45 min during which time the reaction mixture turned cloudy. After cooling to 0 °C, water (150 ml) was added, which led to the formation of a pale pink precipitate. The solids were collected by vacuum filtration, affording a pinkish powder, which was washed with several small portions of water. The supernatant was retained for the isolation of **3** (see below). The solids were dissolved in DCM, dried under vacuum Na_2SO_4, and dried under vacuum to give a red solid (43 mg), comprising a mixture of **5** and **4** (~10%), as determined by ^{1}H NMR spectroscopy. The solids were thoroughly washed with DMF (4 × 0.5 ml), then dried under high vacuum with gentle heating affording **5** as a 5 : 1 ratio of *cis*/*trans* isomers in the form of a pink powder (34 mg, 39%). Single crystals suitable for X-ray diffraction were grown by slow evaporation of a solution in pentane at room temperature.

^{1}H NMR (600 MHz, C_6D_6, 25 °C): δ = 6.23 (dd, $^3J(H_5–H_4)$ = 12 Hz, $^6J(H_5–H_3)$ = 0.5 Hz, 1H, H_5), 5.92 (dd, $^3J(H_4–H_5)$ = 12 Hz, $^5J(H_4–H_3)$ = 0.8 Hz, 1H, H_4), 5.81 (dd, $^3J(H_2–H_1)$ = 4.7 Hz, $^4J(H_2–H_3)$ = 1.1 Hz, 1H, H_2), 4.67 (m, 1H, H_3), 4.16 (d, $^5J(H_1–H_2)$ = 4.7 Hz, H_1), 2.35 (s, 3H, CH_3), 2.29 (s, 6H, N(CH_3)$_2$), 2.24 (s, 3H, CH_3), 2.02 (s, 3H, CH_3), 1.930 (s, 3H, CH_3), 1.926 (s, 3H, CH_3), 1.88 (s, 3H, CH_3), 1.76 (s, 3H, CH_3), 1.721 (s, 3H, CH_3), 1.715 (s, 3H, CH_3), 1.61 (s, 3H, CH_3), 1.57 (s, 6H, CH_3), 1.51 (s, 3H, CH_3), 1.48 (s, 6H, 2 CH_3), 1.46 (s, 3H, CH_3) ppm. ^{13}C NMR (151 MHz, C_6D_6, 25 °C): δ = 150.48 (C_5), 146.88 (C_3), 139.78 (C_6), 130.97 (C_8), 122.15 (C_7), 110.74 (C_2), [89.61, 82.20, 81.75, 81.10, 80.77, 80.47, 80.31, 80.27, 80.25, 80.18, 80.00, 79.68, 79.54, 79.36, 79.01, 78.30, 77.99, 74.65, 74.03, 71.63 (20 *ipso C*'s), 61.21 (C_1), 50.09 (C_4), 43.42 (N(*C*H$_3$)$_2$), 14.28, 11.68, 11.65,

11.40, 10.83, 10.73, 10.36, 10.13, 10.05, 9.98, 9.86, 9.84, 9.56, 9.48, 9.36, 9.18 (Cp-Me's) ppm. IR (ATR): 2963(m), 2941(s), 2902(s), 2853(s), 2813(w), 2767(w), 2713(w), 1741(w), 1684(w), 1652(w), 1615(w), 1595(w), 1564(w), 1465(m), 1444(m), 1431(m) 1377(s), 1316(w), 1301(w), 1277(w), 1248(w), 1230(w), 1207(w), 1186(w), 1149(w), 1092(w), 1067(w), 1027(s), 1007(s), 991(m), 904(w), 872(w), 862(w), 833(w), 821(w), 804(w), 772(w), 754(w), 742(w), 726(m), 688(w), 657(w), 640(w), 622(w), 610(w), 588(w), 580(w), 571(w), 563(w), 549(w), 526(w). MS (APCI+): 738 ([M + H]$^+$, 17%), 693 ([M − Me_2N]$^+$, 100%). HRMS (APCI+): calcd for $C_{46}H_{60}NFe$: 738.3425; found: 738.3428. M.p.: crystalline > 220 °C. We were consistently unable to obtain a satisfactory microanalysis for **5**.

The supernatant from the synthesis of **5** (above) was extracted with 150 ml dichloromethane. The orange organic layer was washed with water (3 × 100 ml) then dried (Na_2SO_4) and evaporated to afford an orange crystalline material (33 mg), containing **3** and **4** in a 1 : 5 ratio and a trace of **5** as determined by ^{1}H NMR spectroscopy. ^{1}H and ^{13}C NMR spectroscopic data for compound **3** were in agreement with the literature.[19]

6: Compound **4** (35 mg, 0.1 mmol) was dissolved in 50 ml ^{t}BuOH, 15 ml water was added and the mixture was stirred for 1 h at room temperature. The solution turned from bright orange to a dark reddish colour. Extraction with hexanes (200 ml) afforded a yellow organic phase and a deep purple aqueous phase. The organic phase was washed with water (3 × 100 ml) and dried (Na_2SO_4). The drying agent was rinsed with DCM (~50 ml) until colorless. The combined organic phase was evaporated to afford a pale yellow solid, which was washed with pentane (5 × 2 ml), then dried under high vacuum, affording analytically pure **6** as a yellow-orange powder (19 mg, 56%). ^{1}H NMR (600 MHz, CD_3OD, 25 °C): δ = 6.23 (dd, $^3J(H_2–H_1)$ = 12.5 Hz, $^3J(H_2–H_3)$ = 3.5 Hz, 1H, H_2), 6.14 (dd, $^3J(H_1–H_2)$ = 12.5 Hz, $^4J(H_1–H_3)$ = 2.5 Hz, 1H, H_1), 5.15 (m, 1H, H_3), 1.84 (s, 3H, CH_3), 1.81 (s, 3H, CH_3), 1.74 (s, 3H, CH_3), 1.72 (s, 3H, CH_3), 1.69 (s, 3H, CH_3), 1.62 (s, 3H, CH_3), 1.58 (s, 3H, CH_3), 1.55 (s, 3H, CH_3) ppm. ^{13}C NMR (151 MHz, [D_6]DMSO, 25 °C): δ = 202.77 (*C*O), 141.79 (CH═CH), 130.88 (CH═CH), 85.24, 85.01, 83.61, 82.78, 81.96, 80.74, 80.00, 79.38, 79.13, 75.18 (8 *ipso-C*'s), 64.14 (*C*(OH)), 10.39, 10.21, 9.88, 9.16, 9.08, 8.85, 8.80, 8.39 (Cp-Me's) ppm. IR (ATR): 3334(w), 2950(w), 2903(w), 1622(w), 1593(s), 1477(w), 1446(w), 1411(w), 1396(w), 1374(m), 1349(w), 1296(w), 1262(w), 1219(w), 1186(w), 1160(w), 1103(w), 1076(w), 1033(m), 976(m), 945(m), 854(w), 826(w), 788(w), 736(w), 698(w), 667(w), 648(w), 634(w), 596(w), 57(w), 563(w), 548(w), 529(w). MS (APCI+): 381 ([M + H]$^+$, 100%), 363 (18%). HRMS (APCI+): calcd for $C_{22}H_{29}O_2Fe$: 381.1517; found: 381.1515. Elemental analysis (%): calcd for $C_{22}H_{38}O_2Fe$: C 69.48, H 7.42; found: C 69.35, H 7.51. M.p.: sublimed ~180 °C.

Crystallography

The crystal data for **3**, *cis*-**5** and **6** are summarized in Table 3. Crystallographic data were collected on an Oxford Diffraction Gemini diffractometer using Cu Kα radiation at 100(2) K for **3**

Table 3 Details of the X-ray structure determinations

Compound	**3**	*cis*-**5**	**6**
CCDC no.	1528957	1528956	1528955
Empirical formula	$C_{22}H_{28}FeO$	$C_{46}H_{59}Fe_2N$	$C_{22}H_{28}FeO_2$
Formula weight	364.29	737.64	380.29
Temperature/K	100(2)	100(2)	270(2)
Crystal system	Orthorhombic	Monoclinic	Monoclinic
Space group	*Pbca*	$P2_1/c$	$P2_1/n$
a/Å	11.3755(9)	17.2794(9)	7.2649(3)
b/Å	15.528(2)	8.5648(7)	16.7822(6)
c/Å	20.3832(17)	25.8751(13)	15.3281(7)
α/°	90	90	90
β/°	90	93.573(5)	101.019(5)
γ/°	90	90	90
Volume/Å^3	3600.5(6)	3821.9(4)	1834.36(13)
Z	8	4	4
ρ_{calc}/*g* cm^{-3}	1.344	1.282	1.377
μ/mm^{-1}	6.732	6.316	6.674
F(000)	1552.0	1576	808.0
Crystal size/mm^3	0.206 × 0.166 × 0.028	0.478 × 0.046 × 0.024	0.390 × 0.050 × 0.040
Radiation	CuKα (*λ* = 1.54178)	CuKα (*λ* = 1.54184)	CuKα (*λ* = 1.54178)
2*Θ* range for data collection/°	10.572 to 135.628	5.124 to 134.6	7.892 to 134.404
Index ranges	−13 ≤ *h* ≤ 11, −18 ≤ *k* ≤ 16, −24 ≤ *l* ≤ 16	−19 ≤ *h* ≤ 20, −7 ≤ *k* ≤ 10, −30 ≤ *l* ≤ 30	−5 ≤ *h* ≤ 8, −19 ≤ *k* ≤ 19, −18 ≤ *l* ≤ 17
Reflections collected	10 036	35 388	8530
Independent reflections	3201 [R_{int} = 0.0579, R_σ = 0.0913]	6773 [R_{int} = 0.0739, R_σ = 0.1021]	3255 [R_{int} = 0.0536, R_σ = 0.0571]
Data/restraints/parameters	3201/0/225	6773/300/654	3255/0/235
Goodness-of-fit on F^2	1.049	1.042	1.005
Final *R* indexes [*I* > = 2*σ*(*I*)]	R_1 = 0.0629 wR_2 = 0.1628	R_1 = 0.0829, wR_2 = 0.2209	R_1 = 0.0730, wR_2 = 0.1705
Final *R* indices [all data]	R_1 = 0.0876 wR_2 = 0.1854	R_1 = 0.1025 wR_2 = 0.2380	R_1 = 0.0864 wR_2 = 0.1803
Largest diff. peak/hole/e Å^{-3}	0.94/−0.54	1.49/−0.56	1.11/−0.44

and *cis*-**5**. Samples of **6** were degrading at that temperature and hence data was collected at 270(2) K. Following absorption corrections and solution by direct methods, the structures were refined against F^2 with full-matrix least-squares using the program SHELXL-2014.[32] All hydrogen atoms were added at calculated positions and refined by use of riding models with isotropic displacement parameters based on those of the parent atoms. Anisotropic displacement parameters were employed throughout for the non-hydrogen atoms. For compound *cis*-**5** two relatively large peaks and other residual electron density was modelled as the second component of a disordered molecule; site occupancies of the two components refined to 0.889 (4) and its complement. Geometries and isotropic displacement parameters of the minor component were restrained to reasonable values. All hydrogen atoms were added at calculated positions and refined by use of riding models with isotropic displacement parameters based on those of the parent atoms. Anisotropic displacement parameters were employed throughout for the non-hydrogen atoms.

DFT calculations

DFT was employed to determine the relative energies of intermediates along the proposed mechanism. The calculations were undertaken using the familiar B3LYP functional with the 6-31G* basis sets for lighter atoms (hydrogen, carbon, oxygen, nitrogen, and chlorine) while the LANL2DZ basis set incorporating an effective core potential (ECP) was used for iron to reduce the computational burden. Each intermediate was fully optimized using the PCM solvent model for DMF, with Cartesian coordinates for all geometries available in the ESI.† Subsequently a vibrational hessian calculation was employed in order to determine if the structures were minima, transition states, or higher order stationary points on the potential energy surface. Thermodynamic corrections were estimated at a temperature of 333.15 K, in line with the experimental conditions. Data provided here are the enthalpy and free energy changes for each step of the proposed mechanism. All calculations were undertaken using the Gaussian 09 program suite.[33]

Electrochemistry

Cyclic voltammetry measurements were conducted in 0.1 M solutions of Bu_4NPF_6 as supporting electrolyte in dichloromethane with analyte concentrations of 1 mM or 3 mM. Acetylferrocene was chosen as internal standard for **3** and **5**, and decamethylferrocene for **6**. Determined potentials are reported *versus* the Fc/Fc^+ couple ($E_{Fc} = E_{AcFc} - 270$ mV; $E_{Fc} = E_{DmFc} + 480$ mV (ref. 34)). The half-width potentials ($E_{1/2}$) were determined by using middle between anodic (E_{pa}) and cathodic peak potentials (E_{pc}).

Acknowledgements

This research was supported under the Australian Research Council's *Discovery Projects* funding scheme (project number DP 150104117). We acknowledge the facilities and the scientific and technical assistance of the Australian Microscopy and Microanalysis Research Facility at the Centre for Microscopy, Characterization and Analysis, The University of Western Australia, a facility funded by the University, State and Commonwealth Governments. This research was undertaken with the assistance of computational resources from the Pople high-performance computing cluster of the Faculty of Science at the University of Western Australia.

Notes and references

1 P. Nguyen, P. Gómez-Elipe and I. Manners, *Chem. Rev.*, 1999, **99**, 1515–1548.
2 R. A. Musgrave, A. D. Russell and I. Manners, *Organometallics*, 2013, **32**, 5654–5667.
3 T. Ogata, K. Oikawa, T. Fujisawa, S. Motoyama, T. Izumi, A. Kasahara and N. Tanaka, *Bull. Chem. Soc. Jpn.*, 1981, **54**, 3723–3726.
4 G. Jaouen, A. Vessieres and S. Top, *Chem. Soc. Rev.*, 2015, **44**, 8802–8817.
5 J. d. J. Cázares-Marinero, O. Buriez, E. Labbé, S. Top, C. Amatore and G. Jaouen, *Organometallics*, 2013, **32**, 5926–5934.
6 A. Sola, A. Espinosa, A. Tárraga and P. Molina, *Sensors*, 2014, **14**, 14339–14355.
7 R. W. Heo and T. R. Lee, *J. Organomet. Chem.*, 1999, **578**, 31–42.
8 D. E. Herbert, U. F. J. Mayer and I. Manners, *Angew. Chem., Int. Ed.*, 2007, **46**, 5060–5081.
9 H. Braunschweig and T. Kupfer, *Eur. J. Inorg. Chem.*, 2012, **2012**, 1319–1332.
10 H. Bhattacharjee and J. Müller, *Coord. Chem. Rev.*, 2016, **314**, 114–133.
11 H. Schottenberger, J. Lukassser, E. Reichel, A. G. Müller, G. Steiner, H. Kopacka, K. Wurst, K. H. Ongania and K. Kirchner, *J. Organomet. Chem.*, 2001, **637–639**, 558–576.
12 M. Roemer, Y. K. Kang, Y. K. Chung and D. Lentz, *Chem. – Eur. J.*, 2012, **18**, 3371–3389.
13 M. Roemer and D. Lentz, *Eur. J. Inorg. Chem.*, 2008, 4875–4878.
14 E. V. Banide, Y. Ortin, B. Chamiot, A. Cassidy, J. Niehaus, A. Moore, C. M. Seward, H. Müller-Bunz and M. J. McGlinchey, *Organometallics*, 2008, **27**, 4173–4182.
15 R. M. Gleixner, K. M. Joly, M. Tremayne, B. M. Kariuki, L. Male, D. M. Coe and L. R. Cox, *Chem. – Eur. J.*, 2010, **16**, 5769–5777.
16 M. Roemer, D. Heinrich, Y. K. Kang, Y. K. Chung and D. Lentz, *Organometallics*, 2012, **31**, 1500–1510.
17 M. Roemer and D. Lentz, *Chem. Commun.*, 2011, **47**, 7239–7241.
18 M. Malischewski, M. Adelhardt, J. Sutter, K. Meyer and K. Seppelt, *Science*, 2016, **353**, 678–682.
19 J. K. Pudelski and M. R. Callstrom, *Organometallics*, 1994, **13**, 3095–3109.
20 M. Ogasawara, T. Nagano and T. Hayashi, *J. Am. Chem. Soc.*, 2002, **124**, 9068–9069.

21 M. Roemer, B. W. Skelton, M. J. Piggott and G. A. Koutsantonis, *Dalton Trans.*, 2016, **45**, 18817–18821.
22 E. Buncel and E. A. Symons, *J. Chem. Soc. D*, 1970, 164–165.
23 T. H. Vaughn and J. A. Nieuwland, *J. Am. Chem. Soc.*, 1934, **56**, 1207–1209.
24 K. Schlögel and W. Steyrer, *Monatsh. Chem.*, 1965, 1520–1535.
25 F. Makra, J. C. Rohloff, A. V. Muehldorf and J. O. Link, *Tetrahedron Lett.*, 1995, **36**, 6815–6818.
26 G. Erker, M. Riedel, S. Koch, T. Joedicke and E.-U. Wuerthwein, *J. Org. Chem.*, 1995, **60**, 5284–5290.
27 V. López-Carrillo and A. M. Echavarren, *J. Am. Chem. Soc.*, 2010, **132**, 9292–9294.
28 C. Nieto-Oberhuber, P. Pérez-Galán, E. Herrero-Gómez, T. Lauterbach, C. Rodríguez, S. López, C. Bour, A. Rosellón, D. J. Cárdenas and A. M. Echavarren, *J. Am. Chem. Soc.*, 2008, **130**, 269–279.
29 A. J. Bard and L. R. Faulkner, *Electrochemical Methods: Fundamentals and Applications*, John Wiley & Sons, Inc., 2nd edn, 2001.
30 O. V. Dolomanov, L. J. Bourhis, R. J. Gildea, J. A. K. Howard and H. Puschmann, *J. Appl. Crystallogr.*, 2009, **42**, 339–341.
31 G. R. Fulmer, A. J. M. Miller, N. H. Sherden, H. E. Gottlieb, A. Nudelman, B. M. Stoltz, J. E. Bercaw and K. I. Goldberg, *Organometallics*, 2010, **29**, 2176–2179.
32 G. M. Sheldrick, *Acta Crystallogr., Sect. C: Cryst. Struct. Commun.*, 2015, **71**, 3–8.
33 M. J. Frisch, *et al.*, *Gaussian 09, Revision B.01*, 2009.
34 N. G. Connelly and W. E. Geiger, *Chem. Rev.*, 1996, **96**, 877–910.